Advances in Colloid and Interface Science
98 (2002) 51–85

ADVANCES IN COLLOID AND INTERFACE SCIENCE

www.elsevier.com/locate/cis

Energy of interaction in colloids and its implications in rheological modeling

Daniel Quemada*, Claudio Berli

LBHP, Université Paris VII-CNRS ESA 7057, Case 7056, 2 Place Jussieu, 75251 Paris Cedex 05, France

Abstract

This work deals with the problem of deriving theoretical connections between rheology and interparticle forces in colloidal suspensions. The nature of interparticle forces determines the colloidal structure (crystalline order due to long range repulsive forces, flocculation due to attractive forces, etc.) and hence, the flow behavior of suspensions. The aim of this article is to discuss how these interactions enter the modeling of rheometric functions, in particular, the shear viscosity. In this sense, the main interactions commonly appearing in colloids are reviewed, as well as the role they play in phase transition behavior. Then, a series of approaches relating the interaction potential to viscosity is examined. The results of applying these models to experimental data are also discussed. Finally, examples of viscosity modeling for different interaction potentials are given, by using the structural model proposed previously by the authors. The possibility of relating the flow behavior of colloidal suspensions to the interaction between particles offers new perspectives for the study and technical applications of these systems.

Keywords: Colloidal dispersions; Interaction potentials; Phase transitions; Rheological modeling; Suspension viscosity

Contents

* Corresponding author. Tel.: +33-1-44-27-43-33; fax: +33-1-44-27-43-35.
E-mail address: quemada@ccr.jussieu.fr (D. Quemada).

0001-8686/02/$ - see front matter
PII: S0001-8686(01)00093-8

1. Introduction

During the last decade, significant progress has been made in understanding the effect of the thermodynamic interactions on rheological properties of colloids [1–4]. This progress results from the development of new methods of preparation and characterization, which lead to a more precise quantification of the physico-chemical parameters in the system. Light scattering techniques have played a crucial role in determining characteristic diffusion times [5] and elucidating phase transition behavior [6]. The knowledge of microstructural changes under shear has also been improved by means of optical measurements simultaneous to rheometry [7]. Nevertheless, the absence of appropriate modeling very often results in the lack of quantitative predictions of rheological behavior as a function of the physico-chemical variables. In principle, a model that involves a correct description of the microstructure should allow one to predict the rheological functions starting from the knowledge of the potential energy between particles. The inverse problem is equally interesting: determining the interaction potential from either a flow curve (viscosity) or a dynamic response (elastic modulus) and then using it to predict how concentration, solvent quality or ionic strength influence the rheological functions. In fact, for industrial applications, an appropriate connection between macroscopic

rheology and microstructure is required to design procedures of on-line characterization.

The arrangement of particles in a colloidal dispersion, and hence the mechanical response, is determined by the nature of the interaction forces. The 'microstructure' resulting for a given interaction can be well described in quiescent conditions [2]. For this reason, rigorous calculations of the rheometric functions are limited to situations where the colloidal structure is not affected significantly; that is, the high frequency limit of the dynamic modulus [8,9] and the low shear viscosity [1,10]. Nevertheless, the rheometric function of interest in most of practical situations is the viscosity as a function of shear stress. Since the description of the microstucture under shear flow is rather difficult, this function is generally treated in a phenomenological context, usually on the basis of scaling principles [11–14]. Precisely, the aim of this article is to discuss how the interaction potential enters the viscosity modeling of concentrated suspensions. In this sense, we firstly review the phenomenological models relating viscosity to interparticle forces found in the literature. Then we revise the main features of the model previously proposed by the authors, underlining the differences with other models. It should be noted that calculations from non-equilibrium statistical dynamics clearly involve the pair potential [15,16]. Nevertheless, these methodologies usually demand rather elaborate computations. In contrast, in the present review we consider a group of models useful for practical purposes. The article is organized as follows. Section 2 is devoted to recall the main interparticle forces acting in colloidal systems (DLVO, hydration, depletion and polymer–polymer interactions). The influences of these colloidal interactions on phase transition behavior are reviewed in Section 3 and the connection with the dynamic modulus of the suspension is mentioned in Section 4. In Section 5 we review the approaches relating the viscosity of concentrated dispersions to interparticle forces. Finally, in Section 6, the prediction of the structural model for different systems is analyzed and examples of application are given.

2. Pair interaction energy in colloidal dispersions

2.1. van der Waals interaction

In colloidal systems, the first interaction to be accounted is that resulting from the London–van der Waals dispersion forces. For spherical particles of radius a separated by a center-to-center distance R, the interaction has the following expression [1,17]

$$U_A = -\frac{A_{pmp}}{6}\left[\frac{2a^2}{R^2-4a^2}+\frac{2a^2}{R^2}+\ln\left(\frac{R^2-4a^2}{R^2}\right)\right] \quad (1)$$

where A_{pmp} is the Hamaker constant for two particles acting across the medium. On the basis of the Lifshitz theory, A_{pmp} is always positive for two identical particles, hence the interaction U_A is always attractive [18]. Approximate values of A_{pmp} can be obtained as $A_{pmp}^{1/2} \approx A_{pp}^{1/2} - A_{mm}^{1/2}$, where A_{pp} and A_{mm} are the Hamaker constants of the particle and the medium, respectively [18]. In the case of surfaces with adsorbed layers, for instance polymer covered particles, Eq. (1) can be written in terms of the Hamaker constants of the individual media: core particle, polymer layer and solvent medium [19]. Eq. (1) is inaccurate at $R \gg a$ because of retardation effects; nevertheless this interaction decreases rapidly and is not relatively important at large distances. The van der Waals interaction can be also suppressed by matching the optical indices of particles and solvent [1,18].

2.2. Electric double layer interaction

Electrically charged particles in aqueous media are surrounded by counterions and electrolyte ions, namely, the screening double layer. As two particles approach each other, the overlapping of double layers leads to long-range repulsive forces due to entropic effects [18]. The profile of the interaction depends on the ratio between the particle size and the Debye screening length κ^{-1}. For two identical particles with surface potential ψ_o, the repulsive interaction is [17],

$$U_R = 2\pi\varepsilon\psi_o^2 a(2a/R)\exp[-\kappa(R-2a)]; \quad \kappa a < 5 \tag{2a}$$

$$U_R = 2\pi\varepsilon\psi_o^2 a\ln\{1+\exp[-\kappa(R-2a)]\}; \quad \kappa a > 5 \tag{2b}$$

where ε is the permittivity of the medium, k_B is the Boltzman constant and T is the absolute temperature. For a z–z electrolyte, $\kappa = (\varepsilon k_B T/2z^2e^2n_b)^{-1/2}$ where e is the electronic charge and n_b is the density number of ions in the bulk. For concentrated systems, in addition to all species of added salt, it is required to take into account the charge of counterions that balance the surface charge of colloidal particles. Therefore an effective screening length can be written as follows [1],

$$\kappa_{eff} = \kappa\left(1 - \frac{3Z\phi}{8\pi a^3 z(1-\phi)n_b}\right)^{1/2} \tag{3}$$

In this equation, n_b is referred to the solvent volume (usually, series suspensions are prepared by diluting a concentrated suspension with the solution used as dialyzate [20]). The second term between brackets in Eq. (3) represents the contribution of counterions, where Z is the mean number of charges per particle and the factor $(1-\phi)$ accounts for the reduced volume available to electrolyte due to the presence of particles. Also the surface potential can be expressed in terms of the surface charge as, $\psi_o = Ze/4\pi\varepsilon a(1+\kappa a)$. Thus, the mean number of charges Z is usually taken as an adjustable parameter to fit experimental results [6,21,22].

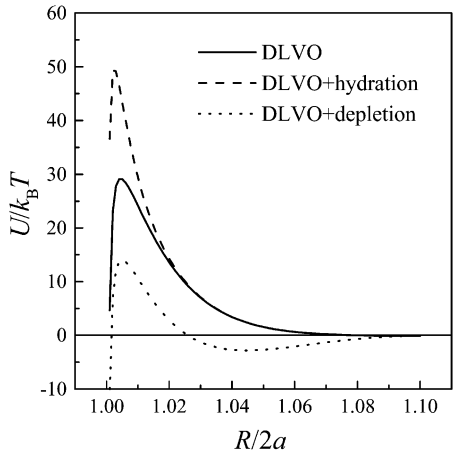

Fig. 1. Dimensionless pair potential as a function of the relative center-to-center distance between particles. Data for numerical calculations are: Eq. (1), $A_{pmp} = 4 \times 10^{-21}$ J; Eq. (2b), $a = 100$ nm, $\psi_o = 25$ mV, $\kappa a = 35$, $\varepsilon = 7.08 \times 10^{-10}$ C^2/Nm^2, $T = 293$ K; Eq. (4), $\Delta G_{pwp} = 0.5$ mJ m^2, $\lambda = 1$ nm; Eq. (5), $\Pi = 10^3$ Pa, $\delta/a = 0.1$.

Other expressions for U_R and ψ_o were proposed in the literature [1,17]. The combination of Eq. (1) with either Eq. (2a) or Eq. (2b) constitutes the well-known DLVO theory for the interaction in charged colloids. Fig. 1 shows schematically the potential curves predicted by these equations.

2.3. Hydrophilic interaction

Here we include the hydration repulsive forces, also called structural forces, which are relevant for several systems in aqueous media [23,24]. The interaction arises from highly hydrophilic surfaces that cause molecular order in the adjacent and neighboring water molecules. This superficial hydration leads to a repulsive force between surfaces, which decays exponentially with a characteristic length $\lambda \approx 1$ nm [18,25]. The corresponding interaction energy for spherical particles can be obtained through the Derjaguin approximation [17,18]. The result is,

$$U_S = \Delta G_{pwp} \pi a \lambda \exp[-(R - 2a)/\lambda] \quad (4)$$

where ΔG_{pwp} is the free energy of interaction between two particles in water [24]. This short-range interaction contributes significantly to the total pair potential of proteins, mica, silice and clay particles [17,18]. In fact, a combination of DLVO and hydration forces (Fig. 1) have been used in the recent literature to interpret direct measurements of the forces between protein-covered oil droplets [26] and rheology of protein [27,28] and clay suspensions [29].

2.4. Depletion interaction

When macromolecules are added to a suspension of colloidal particles, an attractive interaction is generally observed. The mechanism involved is either bridging or depletion, depending on the net interaction between the particles, the macromolecules and the solvent [1,17,18]. In fact, if the polymer chains are able to adsorb onto particle surfaces, and if there exists free binding sites on the opposite surfaces, allowing bridging attraction to occur [18]. This interaction is exponentially decaying with a characteristic distance of the order of the segment polymer length [30]. Nevertheless, if particles are fully covered by the adsorbed polymer the interaction is mainly repulsive (see next section). On the other hand, non-absorbing polymers are excluded from particle surfaces. Thus, if particles are relatively large compared with the polymer, attractive particle–particle forces arise by the mechanism of depletion [1,17,18].

Different approaches have been proposed to explain depletion interaction in colloidal dispersions [31]. Here we consider the exclusion volume theory derived by Asakura and Oosawa [32], which has been proven to be useful for different systems [22,26,33–39]. In this theory, the depleting species are assumed to have an equivalent-hard sphere radius δ and, consequently, to be completely excluded from the gap between particles when $R < 2(a + \delta)$ (see Fig. 2). Thus, there is a depletion layer of thickness δ surrounding the particles (this is in contrast with the theory of de Gennes [40] which considers the depleting species as flexible polymer chains and hence the existence of a polymer density profile next to particle surfaces). The difference in the osmotic pressures between the depleted zone and the bulk solution leads to an attractive interaction between particles, which is written as follows [22,31],

$$U_D = \begin{cases} -\dfrac{4\pi}{3}(a+\delta)^3\left(1 - \dfrac{3R}{4(a+\delta)} + \dfrac{R^3}{16(a+\delta)^3}\right)\Pi; & R < 2(a+\delta) \\ 0; & R \geq 2(a+\delta) \end{cases} \quad (5)$$

For ideal solutions, the osmotic pressure of the bulk is $\Pi = \rho k_B T$, where ρ is the number density of macromolecules. An extension of the van't Hoff equation can be used to account for the non-ideality of the polymer solution [41]. Assuming, as mentioned above, that the depleting species are spherical, the second virial coefficient is four times the volume of the macromolecule. Then the following expression can be written (see also, [34,35])

$$\Pi = \rho k_B T(1 + 2nM/\rho_m N_A) \quad (6)$$

where N_A is the Avogadro number, M is the mean molecular weight of polymer and ρ_m its mass density. In addition, it is suggested in the literature that the depletion potential varies with salt concentration when the depleting species are electrostatically charged [42–45]. The effect arises mainly through the ionic strength

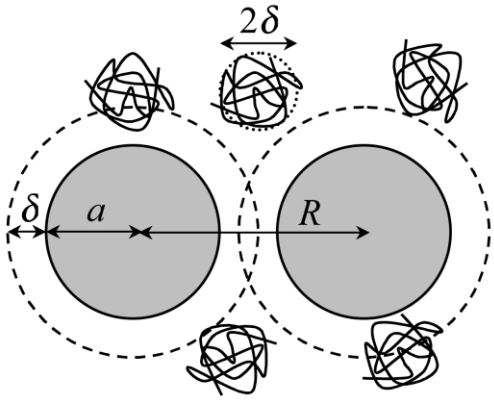

Fig. 2. Schematic representation of a pair of particles of radius a and depleting species of exclusion radius δ.

dependence of the exclusion thickness δ. To take this effect into account, we suggested an effective exclusion radius as follows [39],

$$\delta \approx r_g + b\kappa^{-1} \tag{7}$$

where r_g is the average radius of gyration of polymer and b is a constant (a proportionality between δ and κ^{-1} has been suggested elsewhere [43]). Finally, assuming the additivity of DLVO and depletion forces, the total particle–particle interaction can be calculated by using Eqs. (1), (2a), (2b) and (5). As shown in Fig. 1, the attractive depletion interaction may yield a secondary minimum in the potential curve. Thus, depletion interaction generally leads to weakly flocculated suspensions.

2.5. Polymer–polymer interaction in good solvents

This interaction is common to several colloidal systems such as those containing polymer-covered particles (grafted or adsorbed), microgels and star polymers. As shown schematically in the inset of Fig. 3, L is the thickness of the layer formed by the polymer chains attached to the core and $h = R - 2a$ is the surface-to-surface distance between cores. Polymer is usually added to stabilize the suspensions: if the thickness L is large enough, the van der Waals attraction between cores is negligible in comparison to the Brownian thermal energy. This is the origin of the term 'steric' stabilization [46,47]. Indeed, the overlap of polymer layers reduces the volume available to each single chain, and hence increases the free energy ΔG, producing a repulsive force between particles. The sign of the interaction is, however, governed by the Flory–Huggins interaction parameter, χ, which measures the affinity between the solvent and the polymer chains [48]. According to the description of Napper [47], the free energy of mixture involves the proportionality,

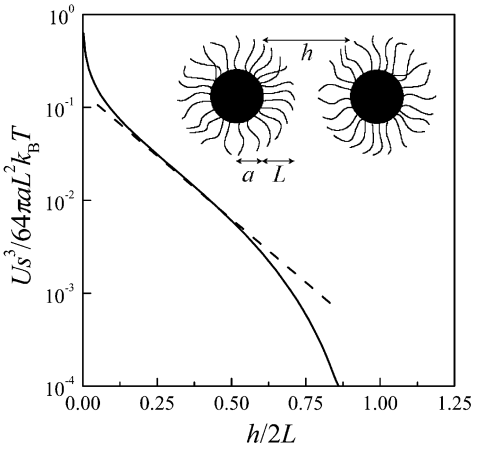

Fig. 3. Dimensionless pair potential as a function of the relative surface-to-surface distance between particles. The full line represents the theory of de Gennes [Eq. (8)]. The dashed line, whose slope is -2π, is the exponential approximation [Eq. (9)]. Inset: schematic representation of a pair of polymer-covered particles.

$\Delta G/k_BT \propto (1/2 - \chi)$. So the interaction is repulsive in good solvents, for which $\chi < 1/2$. In contrast, in poor solvents ($\chi > 1/2$) an attractive interaction arises. In order to control particle aggregation, χ is usually varied by changing the solvent [49], the pH [50] or the temperature [51]. In fact, the adhesiveness of particles strongly depends on temperature, and this effect directly influences rheology [51,52].

The repulsive interaction between polymer 'brushes' in good solvents has been studied by means of both experimental and theoretical methods [1,18,46,47,53–56]. Here we consider the interaction energy between polymer-covered flat surfaces derived by de Gennes [54], which accounts for the osmotic repulsion between polymer layers and the elastic energy of the chains. In particular, the interaction law decays rapidly with distance and it vanishes at $h \geq 2L$. Therefore, the interaction potential between spherical particles can be obtained accurately by using the Derjaguin approximation [57]. The following expression results in [14],

$$U_P = \frac{64\pi aL^2k_BT}{s^3}\left[\frac{1}{5}\left(\frac{h}{2L}\right)^{-1/4} - \frac{1}{77}\left(\frac{h}{2L}\right)^{11/4} + \frac{3}{35}\left(\frac{h}{2L}\right) - \frac{3}{11}\right] \tag{8}$$

where s is the mean distance between the chain attachment points at the core surface. The profile of the interaction predicted by Eq. (8) is presented in Fig. 3. For practical purposes, one may also follow the suggestion of Israelachvili [18], i.e. the interaction energy is roughly exponential and can be written,

$$U_P \approx A_Pk_BT\exp(-\pi h/L) \tag{9}$$

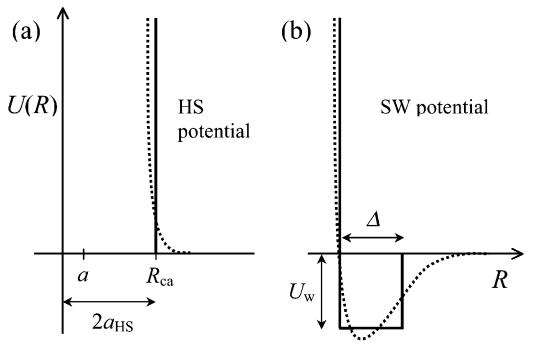

Fig. 4. Diagrams of the simplified interactions: (a) hard sphere potential; (b) square well potential. The dashed lines represent the 'true' pair potentials.

where $A_P \approx 100aL^2/\pi s^3$ (see also [56]). Similar results were reported for the interaction between star polymers [58]. The prediction of Eq. (9) is also drawn in Fig. 3 (dashed line). A good agreement is observed, except for the limits corresponding to very low and very high polymer layer overlapping.

2.6. Simplified forms for potentials

2.6.1. Hard sphere potential

Particles interacting through purely repulsive potentials behave as equivalent-hard spheres (HS). In fact, particles cannot approach each other more than a certain distance, due to the strongly repulsive forces between them. It is then thought that there exists a cut-off potential at $R = R_{ca}$, as shown in Fig. 4a. This distance of closest approach, R_{ca}, defines an equivalent-HS radius, $a_{HS} = R_{ca}/2$ (Fig. 4a). Thus, the HS potential is written,

$$U_{HS} = \begin{cases} +\infty; & R \le 2a_{HS} \\ 0; & R > 2a_{HS} \end{cases} \tag{10}$$

The most appropriate way to calculate a_{HS} is the perturbation theory for molecular liquids developed by Barker–Henderson [59]. This theory provides,

$$a_{BH} = a + \frac{1}{2}\int_{2a}^{\infty}[1 - \exp(-U(R)/k_BT)]\mathrm{d}R \tag{11}$$

where $U(R)$ is the repulsive part of the pair potential. Corrections to the Barker–Henderson model have been proposed in the literature [60–62] in order to add a concentration-dependence to the reference HS radius. Alternatively, in the

case of electrostatic repulsion, an effective HS radius was derived by Russel [63,64] from the dimensional analysis of the conservation equation for the pair distribution of particles. In the limit of very low shear rates, the results is,

$$a_R = \frac{1}{2}\kappa^{-1}\ln\{\alpha/\ln[\alpha/\ln(\alpha/\ldots)]\}; \quad \kappa a \ll 1 \tag{12}$$

where $\alpha = 4\pi\varepsilon\psi_o^2 a^2 \kappa \exp(2\kappa a)/k_B T$. This equation is valid for systems with thick double layers. For thin double layers, the inclusion of the appropriate expression for interparticle forces into the conservation equation leads to [65],

$$a_Q = a + \frac{1}{2}\kappa^{-1}\ln\alpha'; \quad \kappa a \gg 1 \tag{13}$$

with $\alpha' = 32\pi\varepsilon k_B T \kappa a (ze)^{-2}\ tgh^2(ze\psi_o/k_B T)$. Putting $\ln\alpha'/2 \approx b$, one obtains Eq. (7), which expresses the underlying idea that the thickness of the exclusion layer is of the order of the screening length. Finally, it should be said that the HS potential works well for steeply decaying interactions such as steric or strongly screened DLVO interactions (high ionic strength). On the contrary, for electrostatic stabilized systems at low ionic strength, the potential curve decays slowly and the equivalent HS diameter is difficult to determine (see Section 6.3). Particles interacting through such 'soft' potentials are then called 'soft spheres'.

2.6.2. Square well potential

One may also write simplifications for systems in which, in addition to the HS repulsion, a weak remaining attraction is present. In fact, if the range of the interaction potential is short compared to the particle radius, details of the potential curve are not important and particles behave simply as sticky or adhesive hard spheres (AHS). The interaction is described through the square well (SW) potential [66],

$$U_{SW} = \begin{cases} +\infty; & R \le 2a_{HS} \\ -U_w; & 2a_{HS} < R \le 2a_{HS} + \Delta \\ 0; & R > 2a_{HS} + \Delta \end{cases} \tag{14}$$

where the width Δ measures the range of the interaction and the well-depth U_w represents the magnitude of the attractive energy (Fig. 4b). This potential, as well as the limiting form defined by Baxter [67], is widely used to interpret structure [68], phase transition [69], particle diffusivity [70] and rheology [52,71,72] of polymer-covered colloids. In these works, the magnitude of U_w is directly related to the Flory–Huggins parameter χ.

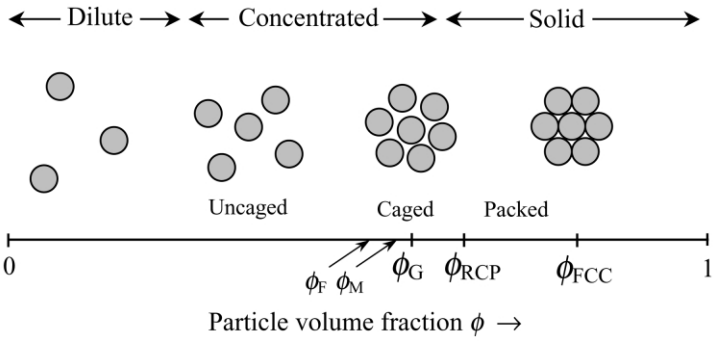

Fig. 5. Schematic 2D-diagram of the equilibrium distribution of particles in a dispersion of hard spheres. Volume fractions at which transitions arise are: freezing, $\phi_F = 0.494$; melting, $\phi_M = 0.545$; glassy, $\phi_G = 0.58$. Also random close packing, $\phi_{RCP} = 0.637$ and face-centered cubic array, $\phi_{FCC} = 0.74$.

3. Concentration regimes and phase transitions

3.1. General background

As stated by Tadros [3], the first step towards understanding the properties of suspensions is analyzing the distribution of particles in the system. In this sense, it is common to use the pair distribution function $g(R)$ provided by statistical mechanics [1,2]. For the purposes of this article, we shall resume some concepts by using the schematic representation shown in Fig. 5. The model system composed of monodisperse HS of radius a dispersed in a Newtonian fluid of viscosity η_F is considered. The particle arrangements in the system depend on the volume space occupied by the particles in relation to the total volume. Hence, the key parameter characterizing the microstructure is the volume fraction $\phi = n4\pi a^3/3$, where n is the number density of particles.

At low ϕ, the mean distance between particles is large compared to particle radius. Thus, particles are able to move freely throughout the medium driven by Brownian forces. The translational diffusion coefficient is given by the Stokes–Einstein relation, $D_0 = k_B T/6\pi\eta_F a$. This regime ($\phi \rightarrow 0$) is considered as the dilute limit. As ϕ increases, hydrodynamic interactions (i.e. the influence on a 'tagged' particle of the flow field generated by the movements of its neighbors) as well as the probability of collision between particles become important. As a consequence, the Brownian motion of the 'tagged' particle is hindered by the presence of the other ones. This effect is observed through the self-diffusion coefficient, which can be measured in the short- and long-time limits [5]. These limiting coefficients are, D_S^S, representing the local motion of particles over distances smaller than particle radius, and D_S^L, representing the motion over distances equivalent to several particle radius, respectively. Both D_S^S and D_S^L decrease with concentration [73]. In this region the suspension is considered to be concentrated.

At higher ϕ, colloidal suspensions present a thermodynamic phase transition, the

onset of which is the freezing concentration $\phi_F = 0.494$. There is then a coexistence of liquid and colloidal crystals in the region $\phi_F \le \phi \le \phi_M$. Above the melting concentration, $\phi_M = 0.545$, the system is fully crystallized. This behavior has been predicted by computer simulations [74] and then confirmed experimentally [1,75]. At these concentration levels, the motion of individual particles is strongly constrained due to the presence of the neighbors. Hence particles diffuse slowly and a glassy transition occurs when ϕ reaches $\phi_G = 0.58$ [76–78]. At this concentration, $D_S^L \to 0$, meaning that each particle is confined into a transient cage formed by its nearest neighbors. The short-time diffusional coefficient remains finite in this region, indicating a vibrational motion of particles within the cage [73]. Furthermore, D_S^S vanishes at $\phi_{RCP} = 0.637$ [10,79,80], the concentration at which the system reaches the random close packing [81]. The suspension concentration could be still increased up to $\phi_{FCC} = 0.74$, where particles become closely packed in a face-centered cubic array. The transitions described above occur at the indicated volume fractions for particles that are *spherical*, *rigid*, *monodisperse* and *without surface forces* (interacting only through hydrodynamics). Polydispersity in size, shape or surface charge, strongly affects the distribution of particles and hence the order–disorder transitions [6,82,83]. It is easily understood that small particles occupy the space among the larger ones, and, at the same time, are more difficult to get entrapped between the neighbors. The overall result is a shift of phase transitions to higher volume fractions.

The main macroscopic feature of the liquid to solid transition in colloidal systems is the divergence of the low shear viscosity η_0. One must comment here that the exact volume fraction at which this rheological response occurs is still a matter of debate in the literature. In the limit of very low shear stress, the distribution of particles is not affected significantly by the viscous forces. Hence, the expectation is that η_0 should diverge at the glass transition [76]; i.e. as $\phi \to 0.58$. This was indeed confirmed in recent measurements on nearly monodisperse HS [84,85]. Nevertheless, former works from de Kruif et al. [86], Jones et al. [87] and Buscall et al. [88] had been shown that η_0 diverges when ϕ approaches 0.63, a value that almost coincides with ϕ_{RCP}. Other works, such as that of Marshall and Zukoski [89], report the divergence of η_0 at $\phi \to 0.6$. The problem is closely related to the concentration dependence of the diffusional coefficient. In fact, the equilibrium distribution of particles after shear perturbation is restored by Brownian motion. Brady [10] argues that, for small departures from equilibrium, the short-diffusivity of particles is sufficient to relax the structure. Thus, the author found, $\eta_0/\eta_F \approx (1 - \phi/\phi_m)^{-2}$, which diverges as $\phi \to \phi_m = \phi_{RCP}$: one factor $(1 - \phi/\phi_m)$ comes from the divergence of $g(R)$ at contact and the other from the vanishing of D_S^S [10]. It is worth noting that the above relation, $\eta(\phi)$, had been found previously [90,91] as the functionality that minimizes the rate of viscous energy dissipation in concentrated suspensions under shear flow. On the other hand, there is important evidence in the literature that the scaling $\eta_0/\eta_F \approx D_0/D_S^L$ holds for concentrated suspensions of HS [80,92–94]. This result suggests that the structural relaxation after shear deformation involves the diffusion of particles over distances higher than the particle radius. Furthermore, since D_S^L vanishes as

$\phi \to \phi_G$, it seems to be theoretically correct that η_0 diverges as ϕ approaches the glass transition [76,85]. The scaling $D_0/D_S^L \sim (1 - \phi/\phi_m)^2 \approx \eta_F/\eta_0$ was also found by Brady [95] from theoretical arguments. Nevertheless, as mentioned above, this author suggests $\phi_m = \phi_{RCP}$. Finally, several reasons may be invoked for the inaccuracies in the experimental determination of the volume fraction at which η_0 diverges: the presence of polydispersity, non-negligible particle–particle interaction, the calculation of ϕ, the goodness of the model $\eta(\phi)$ (if used), or more probable, a combination of these factors (see the discussions in [85] and [89]).

3.2. Effect of interparticle forces

Particle–particle interactions are crucial in determining order and phase transitions. In particular, the presence of long range repulsive forces keep particles apart from one another, leading to crystalline order at low particle concentrations [1]. Furthermore, since diffusivity of particles is strongly diminished, the liquid to solid transition also appears at relatively low volume fractions. In fact, as described in Section 2.6.1, repulsive interactions increase the effective radius of particles up to the HS-like value, a_{HS}, which is half the distance of closest approach. The effective volume fraction is then $\phi_{HS} = \phi(a_{HS}/a)^3 > \phi$. Consequently, the system reaches the glass transition at the critical concentration $\phi^* = \phi_G(a/a_{HS})^3$, i.e. before that the true volume fraction ϕ reaches ϕ_G. This behavior is typically found with charge stabilized particles [1] as well as with polymer-covered particles [75].

Nevertheless, most of phase transitions (and phase *separations*; see [22,37]) found in colloidal systems are due to the presence of attractive forces amongst particles. In fact, attractive potentials yield flocculation and, consequently, formation of particle clusters. At low particle concentrations, clusters are not interconnected and the suspension remains liquid-like. In contrast, above the critical concentration at which the percolation threshold is reached, clusters are interconnected and the system becomes solid-like. The recent work of Weitz and co-workers [96] shows remarkable similarities between the gelation of attractive colloids and the glass transition. As mentioned above, the fluid–solid transition in HS systems occurs when particles get trapped into transient cages and diffusion is no more possible. Similarly, the gelation in aggregating colloids occurs when clusters become crowded. For clusters or radius R_C and fractal dimension d_f [97], the cluster concentration is $\phi_C \approx \phi(R_C/a)^{3-d_f} > \phi$. Thus one can see that the transition occurs at a critical concentration, ϕ^{**}, which is lower than ϕ_G. The value of ϕ^{**} depends on the magnitude of the interaction energy at contact: strong attraction yields clusters loosely packed, so the higher the interaction, the lower the critical concentration for gelation [96]. It is worth noting that in both well-stabilized and aggregating colloids, the critical concentrations at which the liquid–solid transition occurs (ϕ^* and ϕ^{**}, respectively) decrease as the magnitude of the interaction energy increases (repulsive barrier in one case and potential well in the other).

Finally it should be mentioned that strong interparticle forces leading to structural order can be induced by means of external fields [6]. The application of

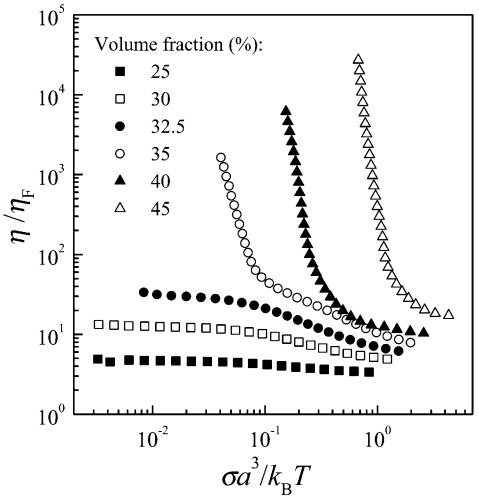

Fig. 6. Relative viscosity, as a function of the dimensionless shear stress, for latices dispersed in water at 20°C. The particle radius is a = 100 nm and the ionic strength is 1 mM (data from Richtering and co-workers [20,152].

electrical or magnetic fields yield the formation of non-isotropic structures in electro- [98] and magneto- [99] rheological fluids, respectively. In both cases, the mechanism involved is the induction of oriented dipole–dipole interactions. Such systems are, however, out of the scope of this review.

3.3. Rheological consequences of phase transitions

Having outlined the sources of phase transitions, following we describe some rheological consequences in the case of well-stabilized suspensions. At low ϕ, the suspension viscosity as a function of shear stress, $\eta(\sigma)$, presents a general shape that involves a low shear Newtonian plateau followed by a shear-thinning region which ends in a second Newtonian plateau at high shear stress. As ϕ approaches ϕ^* the crowding of particles strongly affects the flow behavior of the suspension. Indeed, at $\phi = \phi^*$, the low shear plateau of $\eta(\sigma)$ disappears and, instead of it, an apparent yield stress σ_Y develops. This is a common feature appearing in dispersions of electrically charged latices (Fig. 6), microgels (Fig. 7) and polymerically stabilized particles [11,100,101]. As mentioned above in Section 3.2, the transition occurs long before that the true volume fraction reaches ϕ_G. For the examples shown in Figs. 6 and 7, the critical values are $\phi^* \approx 0.35$ and $\phi^* \approx 0.033$, respectively.

One can see that, for $\phi < \phi^*$, rheology is governed mainly by Brownian motion and the suspension is ‘a liquid’. At concentrations above ϕ^*, rheology is governed by interparticle forces and the suspension behaves virtually as ‘a solid’, presenting

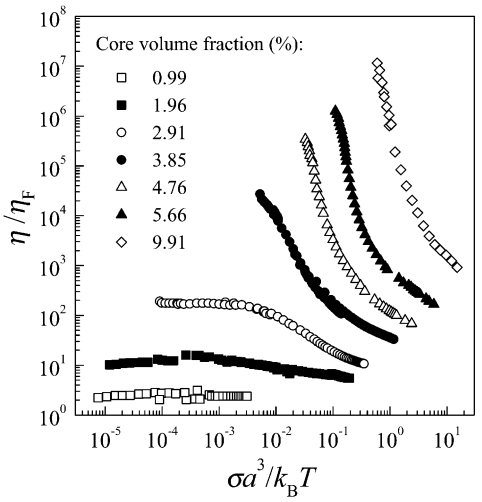

Fig. 7. Relative viscosity, as a function of the dimensionless shear stress, for microgels dispersed in a good solvent at 20°C. The hydrodynamic radius of particles at high dilution is 117 nm (data from Tassin and co-workers [149,150].

elasticity and yield stress. Fig. 8 presents a schematic representation of a stress–concentration phase diagram, which can be obtained by plotting σ_Y as a function of ϕ. The curve of rheometric data defines the transition between the zone of liquid-like behavior (left) and the zone of solid-like behavior (right). The diagram also shows that, for a given volume fraction higher than the critical one, shear stress induces a solid-to-liquid transition. Note that the gradient velocity field can induce further transformations in complex fluids (see, for example, [102,103]). The curve in Fig. 8 can be also drawn from values of the high frequency shear modulus G_∞'. In fact, the ratio σ_Y/G_∞' appears to be nearly constant for different colloidal systems, with values in the range, $0.02 \leq \sigma_Y/G_\infty' \leq 0.04$ [14,104–106]. It is worth noting that the feature presented in Fig. 8 is a general behavior for concentrated suspensions, including aggregating systems [36,107,108] for which the critical value is ϕ^{**}, as discussed above.

4. Relation between the interaction energy and the elastic modulus

Applying small amplitude oscillatory shear perturbs slightly the microstructure and hence the measured shear modulus reflects both the interparticle energy and the structure. In particular, the high frequency limit G_∞' is rather accessible to theoretical treatments and it has been the object of intensive research from several authors. Calculations of G_∞' usually lead to integro-differential equations [8]

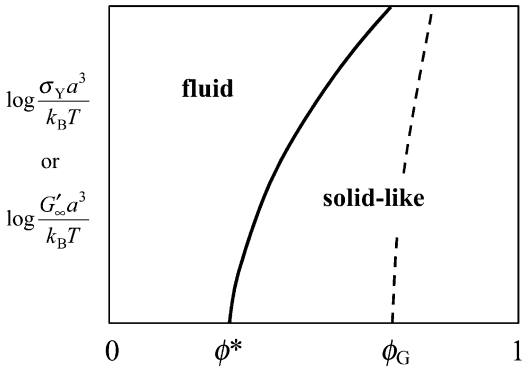

Fig. 8. Schematic representation of the general stress–concentration phase diagram appearing in colloidal dispersions. The full and dashed lines show the transition for repulsive and non-interacting particles, respectively.

involving the interparticle energy $U(R)$ and the pair distribution function $g(R)$, as well as hydrodynamic functions in the more rigorous approaches [16,109]. The expression of Zwanzig and Mountain [8],

$$G_{\infty}^{'} = nk_{\mathrm{B}}T + \frac{2\pi n^2}{15}\int_0^{\infty} g(R)\frac{\mathrm{d}}{\mathrm{d}R}\left(R^4\frac{\partial^2 U(R)}{\partial R^2}\right)\mathrm{d}R, \tag{15}$$

which was derived for molecular fluids, is the common starting point to obtain useful expressions allowing to correlate the modulus G_{∞}' with the potential $U(R)$ in colloids (dispersions of latices, polymerically stabilized particles and microgels). The approximations found in the literature differ from one another mainly in the approximation used to evaluate the pair distribution function. When strongly repulsive forces are present and particles order in a crystalline array, $g(R)$ can be included as a delta function [9,11,110]. For instance, Evans and Lips [110] obtained,

$$G_{\infty}^{'} = nk_{\mathrm{B}}T + \frac{N_{\mathrm{nn}}\phi_{\mathrm{m}}}{5\pi R}\left(\frac{4}{R}\frac{\partial U(R)}{\partial R} + \frac{\partial^2 U(R)}{\partial R^2}\right) \tag{16}$$

where ϕ_{m} is the maximum packing fraction and N_{nn} is the corresponding number of nearest neighbors. The approximations obtained in this way are in excellent agreement with expressions of G_{∞}' derived independently by considering the stress tensor of a crystalline array under small shear deformation [111–113]. Calculations from Eq. (15) were also carried out [20,114] by including $g(R)$ according to the Carnahan and Starling expression [115] with an equivalent-HS volume fraction.

5. Review of viscosity models involving the interaction energy

5.1. Models derived from the classical theory of the activation process

The first attempt grounds on Eyring's theory of rate processes for molecular fluids [116]. Ree and Eyring [117–119] extended this theory to explain shear viscosity of concentrated suspensions. The particle motions are described as jumps from the cage formed by the nearest neighbors to holes into the adjoining cages. The frequency of jumps is $f = f_0\exp(-\Delta U/k_BT)$, where $f_0 \sim D_0/a^2$ and ΔU is the activation energy. Under shear, this frequency is modified due to the shear-induced change of the energy barrier: $\Delta U^* = \Delta U \pm \xi\sigma$. In the term proportional to the stress, the signs − or + account for jumps in or against the flow direction, respectively, and the factor ξ is related to the size of the cage. As the shear rate is proportional to the difference between the frequencies of the two types of jumps, one obtains $\dot\gamma = (1/\beta)\sinh(\xi\sigma/k_BT)$, where $\beta = f_0^{-1}\exp(\Delta U/k_BT)$. Thus, the non-Newtonian viscosity of monomolecular fluids results, $\eta = A\sinh^{-1}(\beta\dot\gamma)/\beta\dot\gamma$, with $A = \beta k_BT/\xi$. For multicomponent systems the authors proposed, $\eta = \sum_i A_i\sinh^{-1}(\beta_i\dot\gamma)/\beta_i\dot\gamma$, where $i = 1,2,\ldots$ identifies each flow unit in the system. In the case of colloidal particles ($i = 1$) and solvent molecules ($i = 2$) one has,

$$\eta = A_1\frac{\sinh^{-1}(\beta_1\dot\gamma)}{\beta_1\dot\gamma} + A_2 \tag{17}$$

since $\beta_2\dot\gamma \ll 1$. Eq. (17) was successfully applied to shear flow data of synthetic rubber latex at different volume fractions and temperatures [120]. A more precise analysis at low shear rates was carried out by using three flow units [121].

Baxter–Drayton and Brady [122] recently applied this theory to model the viscosity of flocculated colloidal dispersions, in particular electro-rheological fluids. Similar arguments on the stress-induced variation of the activation energy barrier lead to,

$$\eta = (\eta_0 - \eta_\infty)\frac{\sinh^{-1}(\beta'\dot\gamma)}{\beta'\dot\gamma} + \eta_\infty \tag{18}$$

where η_0 and η_∞ are the limiting viscosity values for $\dot\gamma \to 0$ and $\dot\gamma \to \infty$, respectively. In contrast to Eq. (17), the relaxation time in Eq. (18) depends on the interaction energy as $\beta' = c(a^2/D_0)(\Delta U/k_BT)^{-1}\exp(\Delta U/k_BT)$, where c is a proportionality constant related to the network structure. This scaling allowed the authors to obtain a single universal curve $\eta = \eta(\beta'\dot\gamma)$. In the framework of Ree–Eyring model, the suspension flows when particles diffuse out of their mutual potential wells. It is noteworthy that the network rearrangement process occurs not on the particle diffusion time scale $f_0^{-1} \sim a^2/D_0$, but on the 'escape time' scale β'.

The model developed by Ogawa et al. [12] considers the shear stress in colloidal suspensions as composed of two terms, the viscous stress σ_v and the particle stress σ_p. The first term is included according to the equation of Krieger [122] [see next

Eq. (22)]. The second term, which involves the interparticle potential, is derived in the context of the activation processes. The relative viscosity is written as follows,

$$\frac{\eta}{\eta_F} = \left(1 - \frac{\phi}{\phi_m}\right)^{-2.5\phi_m} + c_1\phi\exp\left(\frac{\Delta U}{k_B T} - \frac{c_2 d^3\sigma}{\phi k_B T}\right) \tag{19}$$

In the interaction term, c_1 and c_2 (theoretically $\pi/6$) are numerical constants and d is the particle diameter. Also in Eq. (19), the height of energy barrier, ΔU, is taken to be proportional to the pair potential of particles at the mean distance of separation. In the viscous term, $\phi_m = 0.71$ is included to give $\eta_\infty = \eta(\sigma \to \infty)$ in agreement with experimental data for HS [86,87]. In the limit $\sigma \to 0$, one retrieves the model of η_0 proposed early by Goodwin et al. [124]. These authors, however, calculated ΔU as the difference of the total particle potential (considering the nearest neighbors in a face-centered cubic array) between the activated state and the reference state. It is appropriate to remark that in all of the models mentioned above, the interparticle energy arises through a critical shear rate, $\dot{\gamma}_C \approx \beta^{-1}$, similarly to the critical shear stress σ_C in the model derived from structural concepts (see Section 6.3).

In the work of Ogawa et al. [12] it is indicated that, when the effect of repulsive interaction is strong, there is an apparent yield stress given by,

$$\sigma_Y = \frac{\phi U(R)}{c_1 d^3} \tag{20}$$

Although we have not found how to deduce this relation from Eq. (19), Eq. (20) is equivalent to the expression of σ_Y derived by Chen and Zukoski [105]. Actually, by using the mean field potential proposed by these authors, Eq. (20) is easily obtained with $c_1 = 1/3$ instead of $\pi/6$. In fact, the apparent yield stress σ_Y appearing in concentrated colloidal suspensions is related to the interparticle potential. In the case of attractive systems, several expressions relating σ_Y to the energy required to disrupt the aggregates have been proposed in the literature. A detailed description of these models can be found in the review by Tadros [3].

5.2. Models derived from the balance of colloidal forces

As mentioned above in Section 3.1, the dilute regime ends when both hydrodynamic and thermodynamic particle–particle interactions become important. Hence, these interactions enter the Huggins coefficient, k_H, in the virial expansion of the relative viscosity of suspensions [1], that is,

$$\eta/\eta_F = 1 + k_1\phi + k_2\phi^2 + \ldots \tag{21}$$

where $k_1 = 5/2$ and $k_2 = (5/2)^2 k_H$ for spherical particles. Hydrodynamic interactions alone yield $k_2 = 6.2$, as obtained by Batchelor [125]. In addition, k_2 is very sensitive to electrostatic repulsive forces through the second electroviscous effect

[126]. Early attempts to correct k_2 had been made by Blachford et al. [127] by considering the balance between electrostatic and hydrodynamic forces. A more rigorous calculation was made by Russel [63,64], who obtained $k_2 = 2.5 + (3/40)(2a_{eff}/a)^5$, with the effective particle radius a_{eff} given by Eq. (12). The explicit dependence of k_2 with characteristics of the interaction has also been given for suspensions of sticky spheres interacting through SW potentials [71,72].

For concentrated suspensions, the low shear viscosity can be simply obtained by introducing the effective volume fraction $\phi_{eff} = \phi(a_{eff}/a)^3$ in a HS viscosity equation, as for example [123],

$$\frac{\eta}{\eta_F} = \left(1 - \frac{\phi_{eff}}{\phi_m}\right)^{-2.5\phi_m} \tag{22}$$

The effective radius may be calculated from one of the expressions presented in Section 2.6.1. Under finite shear flow, in contrast, hydrodynamic interactions become important in front of electrostatic forces, hence the thermodynamic contribution to viscosity decreases with shear stress. This effect can be accounted by allowing a_{eff} to be shear-dependent [4,11,63,127]. In this context of analysis, Buscall [11,128,129] defined a_{eff} by an extension of Eq. (11),

$$a_{eff} = a + \frac{1}{2}\int_{2a}^{\infty}[1 - \exp(-U(R)/E)]\mathrm{d}R \tag{23}$$

where the collision energy, E, was postulated to be the sum of the thermal and viscous energies,

$$E = k_B T + \sigma a_{eff}^3/K \tag{24}$$

In Eq. (24), $K(\phi_{eff}) = 0.016 + 0.52\phi_{eff}$ is a scaling parameter, the ϕ-dependence of which has been deduced from HS suspension data. An approximate solution of Eq. (23) is obtained if the argument of the exponential is of order one. In this case, the following balance results,

$$\frac{U(R = 2a_{eff})}{k_B T} = k\left(\frac{\sigma a_{eff}^3}{k_B T K(\phi_{eff})} + 1\right) \tag{25}$$

where k ($\approx 1/2$) is a phenomenological factor. The values of $a_{eff}(\phi,\sigma)$, deduced from any given viscosity curve at fixed particle concentration by using Eq. (22), are then introduced into Eq. (25) to obtain an apparent interaction potential $U(\phi,R)$. Therefore, a test for the model is that potential values obtained from different volume fractions should lie on the same potential curve [14,128,129]. Note that in the low shear stress limit, this approximate solution becomes incorrect and the relationship between a_{eff} and $U(R)$ is better stated from Eq. (23). On the other

hand, the yield stress arises in this model if the effective particle radius is high enough to produce dense packing of particles. Therefore, the author suggests,

$$\sigma_Y \approx K(\phi_{eff})\left(\frac{U(R = 2a_m) - k_B T}{a_m^3}\right) \tag{26}$$

where a_m is the maximum radius that particles can take because of spatial constraints. It must be noted here that, in comparison with Eq. (25), Eq. (26) misses the constant k.

This method has been applied to determine an apparent interaction potential of non-aqueous (sterically stabilized) latex. A very satisfactory comparison between predicted viscosity curves and data from Frith [130] has been observed. For the aqueous latex data from Jones et al. [87], only the tail of the potential, not the steep rise for close approach of particles, were available [11]. However, in the case of microgel data from Wolfe and Scopazzi [131], the required superposition of potentials obtained from flow curves at different volume fractions is not attained (see also [14]). Buscall argued that it would be a consequence of the softness of particles which rends the particle radius ϕ-dependent [129]. This method was also used to describe the excess shear-thinning, in comparison with the prediction for HS dispersions, observed in polydisperse emulsions [132].

5.3. Models derived from structural concepts

5.3.1. Main features of structural modeling

It appears important to recall the basic concepts on which this kind of rheological modeling grounds. A further discussion on the kinetic interpretation of non-Newtonian flow can be found in the text of Hunter [2]. In particular, structural models involve: (i) a structural variable S characterizing the structure; (ii) a rate equation of S that accounts for the forces perturbing the microstructure (viscous forces from the gradient velocity field) and those restoring the equilibrium state (Brownian randomizing forces, mainly); and (iii) a given form of the viscosity-structure relation, $\eta(S)$ [133]. In this framework, the well-known models of Krieger–Dougherty [134] and Cross [135] describe the shear-thinning behavior by identifying S to the number of doublets existing under shear or the average number of links per chain of particles, respectively. In both models, the viscosity η is empirically assumed to depend linearly on the structural variable S. Following we discuss the specific definition of S and its relationship with viscosity in the model proposed previously by one of us [136].

The structural state of the dispersion is considered as a mixture of individual particles (IP) and 'groups' of them, hereafter named structural units (SU), suspended in a fluid which contains different species (electrolyte, polymer molecules, etc.). Each SU involves particles that move together, as a coherent cluster, carrying the whole volume of the suspending fluid immobilized. Thus, the shear-thinning behavior is regarded as the result of progressive breakdown of SU, that increases both the total concentration of IP and the total volume of free liquid. Conversely,

shear-thickening behavior is associated to some shear-induced formation of SU. The characteristics of SU (size, shape, shear-dependence, etc.) are very dependent on the type of particle interaction. In the case of attractive forces, SU at rest are flocs, aggregates or clusters of aggregates. Note that in some systems, small aggregates are so rigidly associated (shear forces cannot break down them) that they are considered as IP [137–139]. In the case of repulsive interaction, SU at rest are groups of particles embedded in a suspension of more or less free IP. As mentioned in Section 3, the structure may reach a solid-like state corresponding to a given spatial arrangement of IP. This arrangement, unlikely homogeneous, may be composed of ordered domains (crystallites) separated by desordered fluid [140,141].

Taking ϕ_{SU} and $\phi_{IP} = \phi - \phi_{SU}$ to be the volume fraction of particles contained in all the SU and IP, respectively, the structural variable is defined as the number fraction of particles contained in the whole of SU, i.e. $S = \phi_{SU}/\phi$ [136]. Furthermore, assuming a mean compactness φ into the SU, the effective volume fraction of the disperse phase is $\phi_{eff} = \phi_{SU}/\varphi + \phi_{IP}$. Hence the structural variable enters this definition as

$$\phi_{eff} = \phi(1 + CS) \tag{27}$$

where $C = \varphi^{-1} - 1$ is a compactness factor. Finally, the non-Newtonian viscosity is obtained by introducing Eq. (27) into a well-established equation $\eta(\phi_{eff})$ (see below).

5.3.2. Viscosity model proposed by the authors

As evidence, S depends on shear stress, ranging between the limits $S_0 = S(\sigma \to 0)$ and $S_\infty = S(\sigma \to 0)$. The shear-dependence results from the balance between build-up and breakdown of SU. More precisely, the model considers that the structure is governed by the following relaxation kinetics,

$$\frac{dS}{dt} = -\tau_{hy}^{-1}(S - S_\infty) + \tau_{Br}^{-1}(S_0 - S) \tag{28}$$

where τ_{hy} and τ_{Br} are the characteristic relaxation times of hydrodynamic and Brownian forces, respectively. At a given shear stress σ, the microstructure reaches a dynamical equilibrium and then the steady value of S is given by,

$$\frac{S_0 - S}{S - S_\infty} = \frac{\tau_{hy}^{-1}}{\tau_{Br}^{-1}} \equiv \theta \tag{29}$$

where θ is a kinetic rate ratio. For dilute suspensions of hard spheres the Brownian time scale is $\tau_{Br} \sim a^2/D_0$ which corresponds to the diffusion time of a particle over a distance near its radius. On the other hand, the characteristic time of the hydrodynamic interaction can be seen as the life-time of a doublet rotating in a flow field of shear rate $\dot{\gamma}$ [142], hence one may write $\tau_{hy} \sim \dot{\gamma}^{-1}$. Therefore, for

dilute systems, the kinetic ratio is directly the Péclet number $\mathrm{Pe} = 6\pi\eta_F a^3/k_B T$, which expresses the balance between the work done by viscous forces and Brownian thermal energy.

In concentrated suspensions, the diffusional movement of particles is strongly diminished, hence the medium viscosity η instead η_F is currently considered [101,143]. Thus, the characteristic time scales as $\tau_{Br} \sim \eta a^3/k_B T$ and the kinetic ratio results $\theta \sim \sigma a^3/k_B T$. Writing $\theta = \sigma/\sigma_C$, one defines the critical shear stress of the suspension as $\sigma_C = k_B T/a^3$. This is the well-known scaling for colloidal suspensions of non-interacting particles, where shear forces are in competition with Brownian motion only [123].

The next step in modeling consists in writing an explicit relationship between viscosity and shear stress. Firstly, by introducing Eq. (29) into Eq. (27), the effective volume fraction results,

$$\frac{\phi_{eff}}{\phi_m} = \frac{\phi/\phi_0 + (\phi/\phi_\infty)(\sigma/\sigma_C)}{1 + \sigma/\sigma_C} \tag{30}$$

where $\phi_0 = \phi_m/(1 + CS_0)$ and $\phi_\infty = \phi_m/(1 + CS_\infty)$ are the effective maximum packing fractions corresponding to $\sigma \to 0$ and $\sigma \to \infty$, respectively. Then, the following equation is required,

$$\frac{\eta}{\eta_F} = \left(1 - \frac{\phi_{eff}}{\phi_m}\right)^{-2} \tag{31}$$

which generalizes a relationship between viscosity and volume fraction for concentrated colloidal dispersions [90,91]. Using Eq. (30) into Eq. (31) leads to the following expression [136],

$$\eta(\sigma) = \eta_\infty \left(\frac{1 + \sigma/\sigma_C}{\mathscr{R} + \sigma/\sigma_C}\right)^2 \tag{32}$$

which describes the non-Newtonian behavior of the suspension under steady conditions. In this equation, the rheological index $\mathscr{R}$ is the ratio,

$$\mathscr{R} = \left(\frac{1 - \phi/\phi_0}{1 - \phi/\phi_\infty}\right) = \begin{cases} (\eta_\infty/\eta_0)^{1/2}; & \phi < \phi_0 \\ -\sigma_Y/\sigma_C; & \phi \geq \phi_0 \end{cases} \tag{33}$$

In fact, the model is able to describe the rheological features presented in Section 3.3. That is, for $\phi < \phi_0$ a shear-thinning behavior is observed. As ϕ approaches the critical value $\phi^* \approx \phi_0$, the suspension viscosity diverges and hence an apparent yield stress σ_Y develops. Then a plastic behavior is observed for $\phi > \phi_0$ (see also the work of Zhou et al. [144]). Note that shear-thickening behavior is also predicted for $\mathscr{R} > 1$ [145,146]. Finally one can see that the viscosity model obeys a rheological equation of the form $\eta/\eta_F = f(\phi, \sigma a^3/k_B T)$, as required from the dimensionless analysis of colloidal suspensions [123].

As discussed above, the ratio θ expresses the balance of hydrodynamic interaction energy σa^3 against Brownian thermal energy $k_B T$. Nevertheless, when forces amongst particles are important in comparison with Brownian motion, it is usually thought that the appropriate dimensionless group characterizing the perturbation–relaxation processes involves the interaction energy [3,64,147]. Thus one writes $\sigma a^3/\varepsilon\psi_o^2 a$ in the case of electrostatic repulsion, or simply $\sigma a^3/U_w$ for a suspension particles interacting through a SW potential. Following we describe how the interaction energy U enters the viscosity equation in the structural model. Different situations corresponding to different types of potentials are describe independently.

6. Examples for different interparticle potentials

6.1. Weakly attractive potential

Let us consider particles interacting through potentials with an attractive minimum, such as that resulting from the superposition of DLVO and depletion interactions (Fig. 3), or simply a SW potential (Fig. 4b) for polymer-covered particles in poor solvents. As the potential well is of the order of some $k_B T$ units, these interactions usually lead to reversible flocculation. The shear flow breaks down the aggregates, which are rapidly restored due to the attractive force field. For these systems, it is assumed that the restoration of the structure after a shear deformation depends on interparticle forces in addition to Brownian motion. In this sense, an additional kinetic process of relaxation type is added to the rate equation of S. Thus, Eq. (28) is rewritten as,

$$\frac{dS}{dt} = -\tau_{hy}^{-1}(S - S_\infty) + \tau_{Br}^{-1}(S_0 - S) + \tau_{in}^{-1}(S_0 - S) \tag{34}$$

where τ_{in} is the characteristic relaxation time associated to the interaction potential. In steady conditions ($dS/dt = 0$), Eq. (29) is retrieved, with the kinetic ratio changed into

$$\theta = \tau_{hy}^{-1}/(\tau_{Br}^{-1} + \tau_{in}^{-1})$$

Therefore, it is now necessary to derive a scaling for the relaxation time τ_{in}, in order to write the appropriate expression for the critical shear stress. For this purpose, the following assumptions are made: (a) in a reversible cluster, the particles susceptible to be removed by viscous forces are those in the periphery of the cluster (Fig. 9a). (b) These particles 'feel' a pairwise interaction and, in the equilibrium situation, stay in the minimum of the potential curve at the distance R_m (Fig. 9b). (c) Under flow, shear forces move particles apart a certain distance ΔR. As shown schematically in Fig. 9b, the potential energy of the tagged particle increases up the magnitude ΔU and hence, a restoring force $F_r \approx -\Delta U/\Delta R$

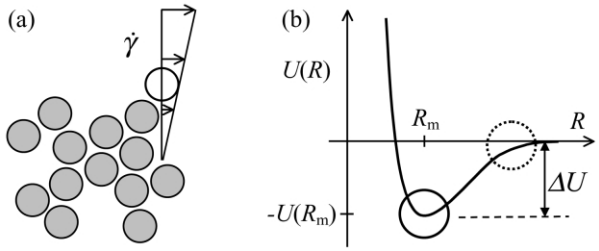

Fig. 9. Schematic representation of particles in a reversible cluster: (a) shear acting on a particle in the cluster border; (b) particle potential energy as a function of distance.

arises. This force is equivalent to that required to remove the particle from the potential well (see also [148]); thus, one may write, $|F_r| \sim U(R_m)/\Delta R$. Assuming further that the particle relaxes through a diffusional movement, the time required to reach the equilibrium position will be proportional to $f_S \Delta R/|F_r|$, where $f_S = 6\pi\eta_F a$ is the Stokes frictional coefficient. If particles move a distance around its radius, one has, $\tau_{in} \sim \eta_F a^3/U(R_m)$. Also for concentrated systems, the suspension viscosity η is included instead of η_F. Finally, the critical shear stress results,

$$\sigma_C = \frac{k_B T}{a^3}\left(1 + \frac{U(R_m)}{k_B T}\right) \tag{35}$$

The viscosity model in this form [Eqs. (32) and (35)] was applied to an oil-in-water emulsion containing sodium caseinate as emulsifier [39]. The oil volume fraction

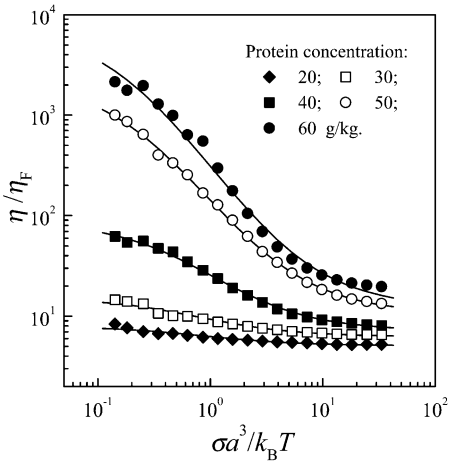

Fig. 10. Relative viscosity of 30% oil-in-water emulsions at 20°C, as a function of the dimensionless shear stress, for different concentrations of sodium caseinate [39]. Full lines represent the viscosity model [Eqs. (32) and (33)].

Table 1
Physicochemical and rheological parameters of 30% oil-in-water emulsions at 20°C, for different concentrations of sodium caseinate [39]

Caseinate (g/kg)	κa	Π (Pa)	η_0 (mPas)	η_∞ (mPas)	σ_C (Pa)	$\frac{U(R_m)}{k_B T}$
20	63	59	17.3	11.1	[0.59]	–
30	77	181	34.5	14.1	[0.59]	–
40	89	309	202	16.7	1.150	0.95
50	99	444	5.3×10^3	25.1	2.082	2.53
60	109	585	18×10^3	30.3	2.976	4.05

Last column is the pair interaction energy at the secondary minimum, as obtained from Eq. (35).

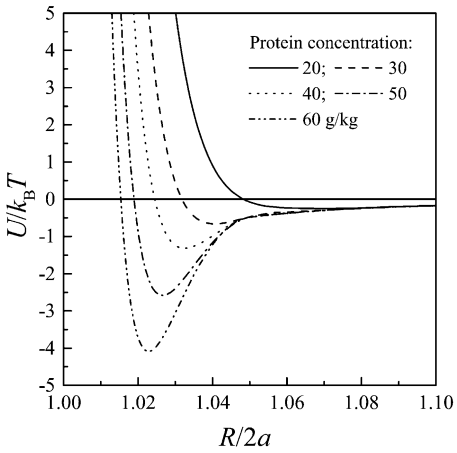

Fig. 11. Dimensionless pair potential as a function of the relative center-to-center distance between droplets. The curves result from the superposition of DLVO and depletion interactions [39]. Data for numerical calculations are: Eq. (1), $A_{pmp} = 4 \times 10^{-21}$ J; Eq. (2b), $a = 190$ nm, $\psi_o = 40$ mV, $\varepsilon = 6.1 \times 10^{-10}$ C^2/Nm^2, $T = 293$ K, κa from Table 1; Eq. (5), Π from Table 1; Eq. (7), $b = 2.55$.

was $\phi = 0.30$ and the equivalent-HS radius of oil droplets was $a = 190$ nm. Different samples were available with sodium caseinate concentration varying between 20 and 60 g/kg. The dimensionless Debye inverse length κa and the osmotic pressure Π of the bulk solution are reported in Table 1. In the aqueous phase, the sodium caseinate forms sub-micelles, which yields reversible droplet–droplet aggregation by the mechanism of depletion. The aggregation increases the effective volume fraction of the disperse phase. Consequently, as can be observed in Fig. 10, the emulsion viscosity increases significantly with the concentration of sodium caseinate. Shear-thinning comes from the gradual breakup of droplet aggregates induced by shear.

The full lines in Fig. 10 represent the viscosity model [Eq. (32)] with the values of η_0, η_∞ and σ_C reported in Table 1. The values of $U(R_m)$ calculated from σ_C using Eq. (35) are also reported in Table 1. As discussed above, these values are assumed to represent the magnitude of the potential well where particles flocculate, namely, the secondary minimum of the potential curve $U(R)$. On the other hand, the theoretical interaction energy between droplets can be predicted as the superposition of DLVO and depletion interaction (see Section 2.4). The calculation uses Eqs. (1), (2b), (5) and (7), with the physicochemical parameters reported in Table 1 (see also the caption of Fig. 11). In Eq. (7), the average radius of sub-micelles is included as $r_g \approx 4.8$ nm and the parameter b is the only unknown in calculations [39]. In fact, $b = 2.55$ was required to predict potential curves with a secondary minimum in agreement with the values of $U(R_m)$ obtained from viscosity (Table 1). The resulting potential curves for different concentrations of sodium caseinate are presented in Fig. 11. One may conclude that the interaction obtained from

rheometric data through the viscosity model are well correlated to the theoretical potential between droplets.

6.2. Steeply decaying repulsive potential

Here we discuss how Eq. (34) is also useful for the case of suspensions containing highly repulsive particles. In particular, microgels dispersed in a good solvent constitute a very illustrative example of particles interacting through a repulsive polymer–polymer potential. This interaction arises at volume fractions beyond the critical one, where $h/2L < 1$ (Section 2.5). The resulting changes in rheology are shown, for example, in Fig. 7. For flow to occur in these systems, an additional energy is required to overcome the repulsive interaction that drives particles away from one another. Consistently, repulsive forces are important to restore the structure after a shear deformation. Therefore, the last term in Eq. (34) accounts for the relaxation of particles due to repulsive interaction. Following it is necessary to infer the relaxation time τ_{in} for these systems.

The simplest assumption considers that each single particle stays in the minimum, $U_{nn}^{(0)}$, of the total potential energy generated by its nearest neighbors, U_{nn}. For the tagged particle shown schematically in Fig. 12a, say particle 1, one has $U_{nn}^{(0)} = \sum_{i=2}^{N_{nn}+1} U(R_{1,i}^{(0)}) \approx N_{nn} U(\bar{R})$, where $\bar{R}$ is the mean distance between particles. Under shear stress, particles are forced to move against the force fields of the other particles. For instance, a tagged particle (Fig. 12a) moves in the r-direction over a distance Δr, however, remaining within the cage formed by the nearest neighbors. The total energy that particle 1 'feels' in this position is, $U_{nn} = \sum_{i=2}^{N_{nn}+1} U(R_{1,i})$. It should be noted here that, although the neighbors also move under shear, a change of the position of particle 1 in relation to the cage is expected. The corresponding change of potential experimented by the tagged particle is, $\Delta U = U_{nn} - U_{nn}^{(0)}$ (Fig. 12b). A very useful simplification arises here for the case of exponentially decaying potentials; that is, $\Delta U \approx pU(\bar{R})$, where p is a numerical constant of the order of one. Thus, the restoring force can be written $|F_r| \sim pU(\bar{R})/\Delta r$. The time required for the particle to reach its equilibrium position after suppressing the shear deformation must be proportional to $f_S \Delta r/|F_r|$ (see also [112]). Therefore, if the particle moves a distance around its radius, the characteristic relaxation time scales as $\tau_{in} \sim \eta_F a^3/U(\bar{R})$. In the case of poly-

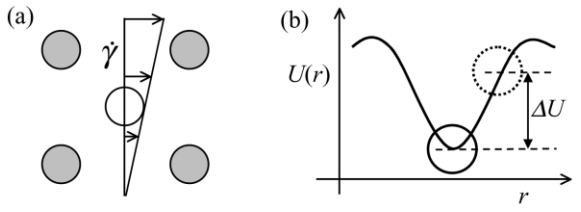

Fig. 12. Schematic representation of particles in a repulsive system: (a) shear acting on a particle in the 'cage'; (b) particle potential energy as a function of distance.

merically stabilized particles and microgels, the effective radius a_{HS} must be considered, which involves the core radius plus the hydrodynamic thickness of the polymer layer [100]. Finally, the critical shear stress results [13],

$$\sigma_C = \frac{k_B T}{a_{HS}^3}\left(1 + \frac{U(\bar{R})}{k_B T}\right) \tag{36}$$

It is important to note that, since $\bar{R} = 2a(\phi_m/\phi)^{1/3}$, the potential curve $U(\bar{R})$ can be obtained from data $\sigma_C(\phi)$, each value of σ_C coming from the curve $\eta(\sigma)$ at a given concentration ϕ.

The viscosity model [Eqs. (32), (33) and (36)], was applied to a system composed of migrogels (copolymer of styrene and acrylic monomers) dispersed in a good solvent (xylene) [13,14]. These microgels were obtained and characterized by Tassin and co-workers [149,150]. In particular, the suspensions studied here contain particles with a core of radius $a \approx 43.5$ nm and a hydrodynamic radius $a_h \approx 117$ nm at infinite dilution. Particles are assumed to have a simple core-shell configuration [150,151]. The core volume fraction is designated ϕ_p and the critical concentration for polymer layer overlapping is $\phi_p^* \approx 3.3\%$. The results of the rheological modeling, which involves the solid–fluid transition, are discussed elsewhere [13]. Here we are mainly concerned with the interaction potential obtained from viscosity data.

Fig. 13 presents the interaction potential (solid circles) obtained from the viscosity curves shown in Fig. 7. Also the calculations of $U(R)$ from different rheometric data, namely dynamic modulus and yield stress, are included for comparison. In fact, the dashed line represent the potential obtained from G_∞' data by using Eq. (16), in which $\phi_m = \phi_{FCC}$ and hence $N_{nn} = 12$ were included. The open circles in Fig. 13 are the prediction of Eq. (20), with $c_1 = \pi/6$, $\phi/d^3 = \phi_p/(2a)^3$, $R = 2a(\phi_m/\phi_p)^{1/3}$ and $\phi_m = 0.71$. In the same figure, the solid line represents Eq. (8), which is deduced from the model of de Gennes. In this equation, $s = 0.36a$ is used, in good agreement with the mean distance between the crosslink points in the microgel particles [14]. One may conclude that the viscosity model predicts the correct form of the interaction potential for microgel suspensions (further comparison with other models is given in Berli and Quemada [14]).

6.3. Soft repulsive potential

The classical approach to interpret the rheology of aqueous suspensions of latices assumes that particles have an effective radius a_{eff}, which involves an exclusion layer of the order of the screening Debye length κ^{-1} (see, for example, [3]). In the following we discuss the main limitations found in applying the equivalent-HS concept to electrically charged particles. Firstly, it is well-known that increasing the particle volume fraction ϕ and/or decreasing the ionic strength yields a liquid–solid transition; that is, the so-called 'colloidal crystal'. Neverthe-

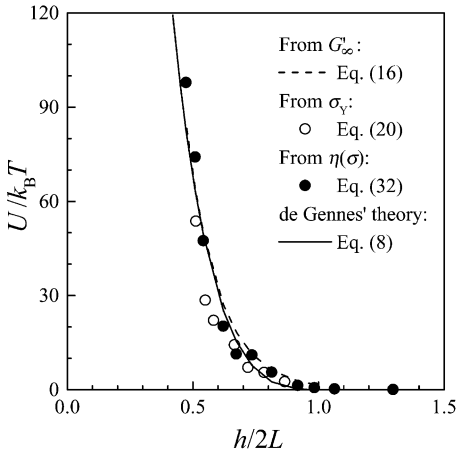

Fig. 13. Dimensionless pair potential as a function of the relative surface-to-surface distance between microgel particles. Each curve corresponds to different rheometric data from the microgel suspension [13,14] (see also the text for details about the models). The full line is the theoretical prediction [Eq. (8) with $s = 0.36a$].

less, ϕ can be increased to values above the critical concentration $\phi^* = \phi_G(a/a_{eff})^3$, resulting in $\phi_{eff} > \phi_{FCC}$ or even $\phi_{eff} > 1$. This fact (the overlapping of the exclusion layers at high concentrations) rends questionable the use of a_{eff} as an equivalent-HS radius. Secondly, under shear stress, particles appear to have a shear-dependent effective radius. The effect is readily observed by analyzing data ϕ_{eff}/ϕ_m vs. σ, which are obtained from experimental data η vs. σ, by using $\phi_{eff}/\phi_m = 1 - (\eta/\eta_F)^{-1/2}$, after inverting Eq. (31). To deduce the equivalent-HS volume fractions in the low ($\phi_{eff,0}$) and high ($\phi_{eff,\infty}$) shear limits, one can include $\phi_m(\sigma \to 0) = 0.58$ (Section 3.2) and $\phi_m(\sigma \to \infty) = 0.71$ [86,87], respectively. The general results is $\phi_{eff,0} \gg \phi_{eff,\infty} \approx \phi$. Correspondingly, one has $a_{eff,0} > a_{eff,\infty} \approx a$. In fact, for $\sigma \to 0$, hydrodynamic forces do not affect appreciably the repulsive interaction, hence $a_{eff,0} \approx a_{HS}$ as defined in Section 2.6.1. For finite values of shear stress, particles can approach each other at distances $R < 2a_{eff,0}$ (the higher the shear stress, the closer the approach, because of the soft character of the repulsive potential). In the limit $\sigma \to \infty$, hydrodynamic forces fully overcome the double layer interaction, allowing particles to approach up to $R \to 2a$. It is then clear that the system should be regarded as a suspension of soft spheres. Nevertheless, up to now, no satisfactory description of $a_{eff} = a_{eff}(\phi,\sigma)$ is available, with the exception of some phenomenological approaches such as that given by Eq. (25).

Following on we present some preliminary results obtained from the analysis of concentrated suspensions of charged latices from Richtering and co-workers [20,152]. In particular, we consider the suspensions containing particles of radius $a = 100$ nm, whose main characteristics are presented in Table 2. Typical curves of the relative viscosity as a function of shear stress are shown in Fig. 6. The DLVO

Table 2
Physicochemical parameters of the latex suspensions at 20°C [20] and theoretical predictions of the equivalent-HS radius, for different values of the ionic strength

Ionic strength (M)	κa	Z	a_{HS}/a	
			Eq. (11)	Eq. (13)
10^{-4}	3.5	380	1.50	1.46
10^{-3}	10.5	1400	1.22	1.19
10^{-2}	33	7350	1.09	1.07

pair potential is presented in Fig. 14 and the prediction of the equivalent-HS radius from both Eqs. (11) and (13) is reported in Table 2 (calculations involve the corresponding values of Z and κa). The relative radius a_{HS}/a represents the interparticle distance $R/2a$ at which $U \approx k_B T$, as indicated by the arrows in Fig. 14. One can readily see that, for the lowest ionic strength, particles with kinetic energy of approximately $3k_B T$, which is easily reached under shear stress, can climb the smooth energy barrier up to $R/2a \approx 1.3$ (Fig. 14). The reduction of the effective radius $a_{eff} \approx R/2a$ means a significant reduction of ϕ_{eff}, which leads to the effects discussed above (the excess shear-thinning in relation to HS systems). In contrast, at high ionic strength the potential decays steeply and the effective radius does not change appreciably. In fact, particles with well-screened potentials behave nearly as HS.

Fig. 15 presents the effective particle radius obtained from the low shear viscosity, i.e. $a_{eff,0}/a = (\phi_{eff,0}/\phi)^{1/3}$ with $\phi_{eff,0}/0.58 = 1 - (\eta_0/\eta_F)^{-1/2}$. As expected, the values obtained from rheology are lower than those predicted theoreti-

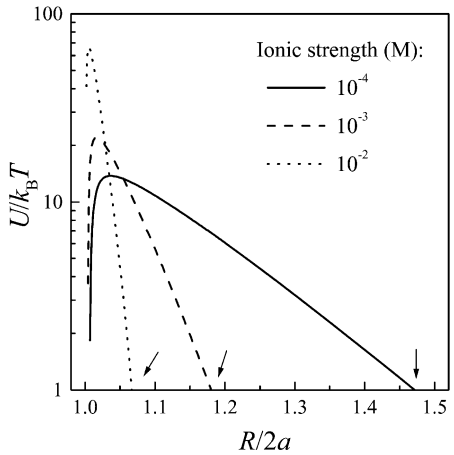

Fig. 14. Dimensionless DLVO pair potential as a function of the relative center-to-center distance between particles. Data for numerical calculations are: Eq. (1), $A_{pmp} = 1.3 \times 10^{-20}$ J; Eqs. (2a) and (2b), $a = 100$ nm, $\varepsilon = 7.08 \times 10^{-10}$ C^2/Nm^2, $T = 293$ K, κa and Z from Table 2.

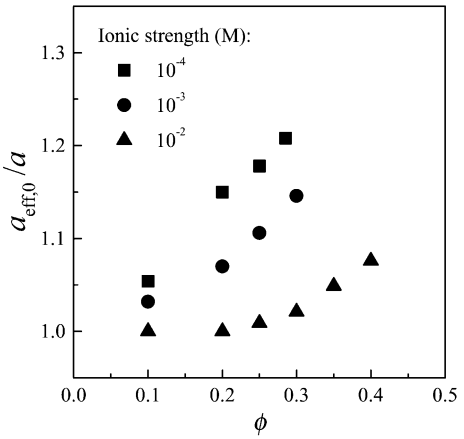

Fig. 15. Effective particle radius (from the low shear plateau, see text for details) as a function of volume fraction, for electrically charged latices at different values of the ionic strength.

cally (Table 2), mainly at the lowest ionic strength. In addition, a clear increase of $a_{\mathrm{eff},0}/a$ with ϕ is observed in Fig. 14. This trend is in contrast with the evolution of $a_{\mathrm{HS}}(\phi)$ expected for concentrated systems [60–62] (one should recall here that Eqs. (11) and (13) apply to dilute systems). This effect probably arises from a variation of Z with ϕ, due to a change of the equilibrium dissociation of acid groups onto particle surfaces [114,153]. Indeed, varying particle concentration modifies the colloid as a whole and, hence, the physicochemical variables cannot be simply extrapolated.

7. Concluding remarks and perspectives

Throughout this article, we have tried to show how colloidal interactions are taken into account in modeling suspension rheology, in order to derive models capable of predicting not only the material response under a given shear condition, but also the effects of the different variables which govern the system. For this reason, a brief analysis of the potentials used to describe particle interactions in colloids has been given. Then, taking HS as the reference system, we revised the variation of microstructure as the particle volume fraction increases. In fact, the analysis of the phase transition phenomena helps one to better understand the corresponding changes in flow behavior. Several models relating viscosity to interparticle forces were analyzed to illustrate the main kind of approaches found in the literature.

In the context of the structural model, special emphasis has been made to the relaxation mechanisms associated to interparticle forces. The derivation of the characteristic relaxation times was explained on the basis of restoring forces and diffusional movement. It has been shown that the model allows one to obtain an

effective potential of interaction directly from the viscosity data. As a consequence, quantitative analysis of the effect of physicochemical variables on the rheology of colloids can be made. For example, in the case of depletion flocculated emulsions, both the osmotic pressure of the bulk solution and the characteristic Debye length (closely related to concentration of depleting species and ions in the bulk, respectively) were well correlated with the characteristics of the viscosity curves.

Additional information can be obtained in the case of repulsive potentials, namely, the interaction energy as a function of interparticle distance. In fact, for microgel suspensions, the interaction potential determined from the viscosity model shows a remarkable agreement with the theoretical prediction for polymer-covered particles. The resulting potential was also cross-checked with that determined from the high frequency shear modulus. On the other hand, apart from the connection to microstructure, the structural model provides a satisfactory description of the viscosity curve of concentrated suspensions presenting liquid–solid transition. The structural relaxation kinetics was also applied recently to interpret rheo-optical measurements [154].

Finally we discussed some questions found in trying to model the rheology of concentrated suspensions of electrically charged latices. In the case of steric stabilization, the abruptness of the interaction potential allows the HS model to work very well. In contrast, in the case of electrostatic stabilization at low ionic strength, the classical definition does not apply due to the smoothness of the potential curve. Indeed, for these systems that behave as suspensions of soft spheres more than HS, modeling the viscosity is still an open problem.

Acknowledgements

C.B. acknowledges receipt of a postdoctoral fellowship from CONICET (Argentina) and educational leave of absence from UNL (Argentina).

References

[1] W.B. Russel, D.A. Saville, W.R. Schowalter, Colloidal Dispersions, 2nd ed., Cambridge University Press, Cambridge, 1991.
[2] R. Hunter, Clarendon Press, Oxford, Foundations of Colloid Science, II, 1992.
[3] Th.F. Tadros, Adv. Colloid Interface Sci. 68 (1996) 97.
[4] R.G. Larson, The Structure and Rheology of Complex Fluids, Oxford University Press, New York, 1999.
[5] J.W. Goodwin, R.H. Ottewill, J. Chem. Soc. Faraday Trans. 87 (1991) 357.
[6] A.K. Arora, B.V.R. Tata, Adv. Colloid Interface Sci. 78 (1998) 49.
[7] N.J. Wagner, Curr. Opin. Colloid Interface Sci. 3 (1998) 391.
[8] R. Zwanzig, R.D. Mountain, J. Chem. Phys. 43 (1965) 4464.
[9] N.J. Wagner, J. Colloid Interface Sci. 161 (1993) 169.
[10] J.F. Brady, J. Chem. Phys. 99 (1993) 567.
[11] R. Buscall, J. Chem. Soc. Faraday Trans. 87 (1991) 1365.
[12] A. Ogawa, H. Yamada, S. Matsuda, K. Okajima, M. Doi, J. Rheol. 41 (1997) 769.
[13] C.L.A. Berli, D. Quemada, Langmuir 16 (2000) 7968.

[14] C.L.A. Berli, D. Quemada, Langmuir 16 (2000) 10509.
[15] W.B. Russel, A.P. Gast, J. Chem. Phys. 84 (1986) 1815.
[16] N.J. Wagner, W.B. Russel, Physica A 155 (1989) 475.
[17] R. Hunter, Clarendon Press, Oxford, Foundations of Colloid Science, I, 1992.
[18] J. Israelachvili, Intermolecular and Surface Forces, 3rd ed., Academic Press, London, 1997.
[19] J. Israelachvili, Proc. R. Soc. Lond. A 331 (1972) 39.
[20] F.M. Horn, W. Richtering, N. Bergenholtz, N. Willenbacher, N.J. Wagner, J. Colloid Interface Sci. 225 (2000) 166.
[21] H.M. Lindsay, P.M. Chaikin, J. Chem. Phys. 76 (1982) 3774.
[22] W.B. Russel, The Dynamics of Colloidal Systems, The University of Wisconsin Press, Madison, 1987.
[23] J. Israelachvili, H. Wennerström, Nature 379 (1996) 219.
[24] C.J. van Oss, Curr. Opin. Colloid Interface Sci. 2 (1997) 503.
[25] C.J. van Oss, Interfacial Forces in Aqueous Media, Marcel Dekker, Inc, New York, 1994.
[26] T.D. Dimitrova, F. Leal-Calderon, Langmuir 15 (1999) 8813.
[27] C.L.A. Berli, J.A. Deiber, M.C. Añón, Food Hydrocoll. 13 (1999) 507.
[28] C.L.A. Berli, J.A. Deiber, M.C. Añón, J. Agric. Food Chem. 47 (3) (1999) 893.
[29] J.D.G. Duran, M.M. Ramos-Tejada, F.J. Arroyo, F. Gonzalez-Caballero, J. Colloid Interface Sci. 229 (2000) 107.
[30] H. Ji, D. Hone, P.A. Pincus, G. Rossi, Macromolecules 23 (1990) 698.
[31] P. Jenkins, M. Snowden, Adv. Colloid Interface Sci. 68 (1996) 57.
[32] S. Asakura, F. Oosawa, J. Polym. Sci. 33 (1958) 183.
[33] H. de Hek, A. Vrij, J. Colloid Interface Sci. 84 (1981) 409.
[34] P.R. Sperry, J. Colloid Interface Sci. 87 (1982) 375.
[35] M. Aronson, Langmuir 5 (1989) 494.
[36] W. Liang, Th.F. Tadros, P.F. Luckham, J. Colloid Interface Sci. 155 (1993) 156.
[37] S.M. Ilet, A. Orrock, W.C.K. Poon, P.N. Pusey, Phys. Rev. E 51 (1995) 1344.
[38] E. Dickinson, M. Golding, J. Colloid Interface Sci. 191 (1997) 166.
[39] C.L.A. Berli, D. Quemada, A. Parker, Colloids Surf. A: Physicochem. Eng. Aspects (2000) submitted.
[40] P.-G. de Gennes, Macromolecules 14 (1981) 1637.
[41] P.C. Hiemenz, Principles of Colloid and Surface Chemistry, Marcel Dekker Inc, New York, 1986.
[42] J. Bibette, D. Roux, B. Pouligny, J. Phys. II 2 (1992) 401.
[43] O. Mondain-Monval, F. Leal-Calderon, J. Bibette, J. Phys. II 6 (1996) 1313.
[44] E.S. Pagac, R.D. Tilton, D.C. Prieve, Langmuir 14 (1998) 5106.
[45] M. Shields, R. Ellis, B. Sounders, Colloids Surf. A: Physicochem. Eng. Aspects 178 (2001) 265.
[46] B. Vincent, Adv. Colloid Interface Sci. 4 (1974) 193.
[47] D.H. Napper, J. Colloid Interface Sci. 58 (1977) 390.
[48] P.J. Flory, Principles of Polymer Chemistry, Cornell Univ. Press, Ithaca, NY, 1953.
[49] S.R. Raghavan, J. Hou, G.L. Baker, S.A. Khan, Langmuir 16 (2000) 1066.
[50] A. Fernández-Nieves, A. Fernández-Barbero, B. Vincent, F.J. de las Nieves, Langmuir 17 (2001) 1841.
[51] M.D. Croucher, T.H. Milkie, Faraday Discuss. Chem. Soc. 76 (1983) 261.
[52] A.T.J.M. Woutersen, J. Mellema, C. Blom, C.G. de Kruif, J. Chem. Phys. 101 (1994) 542.
[53] I. Markovic, R.H. Ottewill, S.M. Underwood, Th.F. Tadros, Langmuir 2 (1986) 625.
[54] P.-G. de Gennes, Adv. Colloid Interface Sci. 27 (1987) 189.
[55] S.T. Milner, T.A. Witten, M.E. Cates, Macromolecules 21 (1988) 2610.
[56] B.A. Costello, P.F. Luckhan, Th.F. Tadros, Langmuir 8 (1992) 464.
[57] L.R. White, J. Colloid Interface Sci. 95 (1983) 286.
[58] C.N. Likos, H. Löwen, M. Watzlawek, B. Abbas, O. Jucknischke, J. Allgaier, D. Richter, Phys. Rev. Lett. 80 (1998) 4450.
[59] J.A. Barker, D. Henderson, J. Chem. Phys. 47 (1967) 2856.
[60] L. Verlet, J.J. Weiss, Phys. Rev. A 5 (1972) 939.
[61] W. van Megen, I. Snook, J. Colloid Interface Sci. 100 (1984) 359.

[62] L.P. Voegtli, C.F. Zukoski, J. Colloid Interface Sci. 141 (1991) 79.
[63] W.B. Russel, J. Fluid Mech. 85 (1978) 209.
[64] W.B. Russel, J. Rheol. 24 (1980) 287.
[65] D. Quemada, Europhys. Lett. 25 (1994) (1994) 149.
[66] J.A. Barker, D. Henderson, J. Chem. Phys. 47 (1967) 4714.
[67] R.J. Baxter, J. Chem. Phys. 49 (1968) 2770.
[68] C. Regnaut, J.C. Ravey, J. Chem. Phys. 91 (1989) 1211.
[69] A. Vrij, M.H.G.M. Pender, P.W. Rouw et al., Faraday Discuss. Chem. Soc. 90 (1990) 31.
[70] P.W. Rouw, C.G. de Kruif, J. Chem. Phys. 88 (1988) 7799.
[71] B. Cichocki, B.U. Felderhoff, J. Chem. Phys. 93 (1990) 4427.
[72] J. Bergenholtz, N.J. Wagner, I EC Process Des. Dev. R 33 (1994) 2391.
[73] R.H. Ottewill, N.St.J. Williams, Nature 325 (1987) 232.
[74] W.G. Hoover, F.H. Ree, J. Chem. Phys. 49 (1968) 3609.
[75] P.N. Pusey, W. van Megen, Nature 320 (1986) 340.
[76] L.V. Woodcock, Adv. Chem. Phys. 48 (1981) 397.
[77] P.N. Pusey, W. van Megen, Phys. Rev. Lett. 59 (1987) 2083.
[78] W. van Megen, S.M. Underwood, Phys. Rev. E 49 (1994) 4206.
[79] P.N. Segrè, O.P. Behrend, P.N. Pusey, Phys. Rev. E 52 (1995) 5070.
[80] P.N. Segrè, S.P. Meeker, P.N. Pusey, W.C.K. Poon, Phys. Rev. Lett. 75 (1995) 958.
[81] D.G. Scott, Nature 188 (1960) 908.
[82] S.I. Henderson, T.C. Mortensen, S.M. Underwood, W. van Megen, Physica A 233 (1996) 102.
[83] P.N. Pusey, J. Phys. 48 (1987) 709.
[84] S-E. Phan, W.B. Russel, Z. Cheng et al., Phys. Rev. E 54 (1996) 6633.
[85] S.P. Meeker, W.C.K. Poon, P.N. Pusey, Phys. Rev. E 55 (1995) 5718.
[86] C.G. de Kruif, E.M.F. van Iersel, A. Vrij, W.B. Russel, J. Chem. Phys. 83 (1985) 4717.
[87] D.A.R. Jones, B. Leary, D.V. Boger, J. Colloid Interface Sci. 147 (1991) 479.
[88] R. Buscall, P. D'Haene, J. Mewis, Langmuir 10 (1994) 1439.
[89] L. Marshall, C.F. Zukoski, J. Phys. Chem. 94 (1990) 1164.
[90] D. Quemada, Rheol. Acta 16 (1977) 82.
[91] D. Quemada, in: J. Casas-Vasquez, G. Lebon (Eds.), Lecture Notes in Physics 164, Springer-Verlag, Berlin, 1982.
[92] A. van Vlaaderen, J. Peetermans, G. Maret, J.K.G Dhont, J. Chem. Phys. 96 (1992) 4591.
[93] A. Imhof, A. van Blaaderen, G. Maret, J. Mellema, J.K.G. Dhont, J. Chem. Phys. 100 (1994) 2170.
[94] G.H. Koenderink, A.P. Philipse, Langmuir 16 (2000) 5631.
[95] J.F. Brady, J. Fluid Mech. 272 (1994) 109.
[96] P.N. Segrè, V. Prasard, A.B. Schofield, D.A. Weitz, Phys. Rev. Lett. 86 (2001) in press.
[97] M.Y. Lin, H.M. Lindsay, D.A. Weitz, R.C. Ball, R. Klein, P. Makin, Nature 339 (1989) 360.
[98] T. Halsey, Science 258 (1992) 761.
[99] N. Buske, H. Sonntag, T. Götze, Colloids Surf. 12 (1984) 195.
[100] G.N. Choi, I.M. Krieger, J. Colloid Interface Sci. 113 (1986) 101.
[101] J. Mewis, W.J. Frith, T.A. Strivens, W.B. Russel, AIChE J. 35 (1989) 415.
[102] R.G. Larson, Rheol. Acta 31 (1992) 497.
[103] P. Buttler, Curr. Opin. Colloid Interface Sci. 4 (1999) 214.
[104] R. Buscall, J.W. Goodwin, M.W. Hawkins, R.H. Ottewill, J. Chem. Soc. Faraday Trans. I 78 (1982) 2873.
[105] L.-B. Chen, C.F. Zukoski, J. Chem. Soc. Faraday Trans. 86 (1990) 2629.
[106] M.E. Fagan, C.F. Zukoski, J. Rheol. 41 (1997) 373.
[107] J.W. Goodwin, R.W. Hughes, S.J. Partridge, C.F. Zukoski, J. Chem. Phys. 85 (1986) 559.
[108] R. Buscall, I.J. McGowan, C.A. Mumme-Young, Faraday Discuss. Chem. Soc. 90 (1990) 115.
[109] L. Elliot, W.B. Russel, J. Rheol. 42 (1998) 361.
[110] D. Evans, A.J. Lips, Chem. Soc. Faraday Trans. 86 (1990) 3413.
[111] B. van der Vorst, D. van den Ende, J. Mellema, J. Rheol. 39 (1995) 1183.

[112] R. Buscall, J.W. Goodwin, M.W. Hawkins, R.H. Ottewill, J. Chem. Soc. Faraday Trans. I 78 (1982) 2889.
[113] J.W. Goodwin, T. Gregory, J.A. Miles, B.C.H. Warren, J. Colloid Interface Sci. 97 (1984) 488.
[114] J. Bergenholtz, N. Willenbacher, N.J. Wagner, B. Morrison, D. van den Ende, J. Mellema, J. Colloid Interface Sci. 202 (1998) 430.
[115] N.F. Carlahan, K.E. Starling, J. Chem. Phys. 51 (1969) 635.
[116] S. Glasstone, K.J. Laidler, H. Eyring, The Theory of the Rate Processes, McGraw-Hill, New York, 1941.
[117] T. Ree, H. Eyring, J. Appl. Phys. 26 (1955) 793.
[118] T. Ree, H. Eyring, J. Appl. Phys. 26 (1955) 800.
[119] T. Ree, H. Eyring, in: F. Eirich (Ed.), Rheology 2, Academic Press, London, 1958.
[120] S.H. Maron, P.E. Pierce, J. Colloid Sci. 11 (1956) 80.
[121] S.H. Maron, A.W. Sisko, J. Colloid Sci. 12 (1957) 99.
[122] Y. Baxter-Drayton, J.F. Brady, J. Rheol. 40 (1996) 1027.
[123] I.M. Krieger, Adv. Colloid Interface Sci. 3 (1972) 111.
[124] J.W. Goodwin, T. Gregory, J.A. Stile, Adv. Colloid Interface Sci. 17 (1982) 185.
[125] G.K. Batchelor, J. Fluid Mech. 83 (1977) 97.
[126] B. Conway, A. Dobry-Duclaux, in: F. Eirich (Ed.), Rheology 3, Academic Press, London, 1960.
[127] J. Blachford, F.S. Chan, D.A.I. Goring, J. Phys. Chem. 73 (1969) 1062.
[128] R. Buscall, Langmuir 8 (1992) 2077.
[129] R. Buscall, Colloids Surfaces A 83 (1994) 33.
[130] W.J. Frith, T.A. Strivens, J. Mewis, J. Colloid Interface Sci. 139 (1990) 55.
[131] M.S. Wolfe, C. Scopazzi, J. Colloid Interface Sci. 133 (1989) 265.
[132] A.M. Howe, A. Clarke, Langmuir 13 (1997) 2617.
[133] D.C.-H. Cheng, F. Evans, Br. J. Appl. Phys. 16 (1965) 1599.
[134] I.M. Krieger, T.J. Dougherty, Trans. Soc. Rheol. 3 (1959) 137.
[135] M.M. Cross, J. Colloid Sci. 20 (1965) 417.
[136] D. Quemada, Eur. Phys. J. AP 1 (1998) 119.
[137] A.S. Michaels, J.C. Bolger, Ind. Eng. Chem. Fund. 1 (1962) 24.
[138] A.S. Michaels, J.C. Bolger, Ind. Eng. Chem. Fund. 1 (1962) 153.
[139] V. Trappe, D.A. Weitz, Phys. Rev. Lett. 85 (2000) 449.
[140] B. van der Vorst, D. van den Ende, N.J.J. Aelmans, J. Mellema, Phys. Rev. E 56 (1997) 3119.
[141] B. van der Vorst, D. van den Ende, N.A. Takin, J. Mellema, Phys. Rev. E 57 (1998) 3115.
[142] H. Goldsmith, S. Mason, in: F. Eirich (Ed.), Rheology 4, Academic Press, London, 1967.
[143] D. Quemada, Rheol. Acta 17 (1978) 632.
[144] J.Z.K. Zhou, T. Fang, G. Luo, P.H.T. Uhlherr, Rheol. Acta 34 (1995) 544.
[145] D. Quemada, Eur. Phys. J. AP 2 (1998) 175.
[146] D. Quemada, Eur. Phys. J. AP 3 (1999) 309.
[147] D. Quemada, Progr. Colloid Polym. Sci. 79 (1989) 112.
[148] R. de Roij, A.A. Potanin, D. van den Ende, J. Mellema, J. Chem. Phys. 99 (1993) 9213.
[149] C. Raquois, J.F. Tassin, S. Rezaiguia, A.V. Gindre, Prog. Organic Coatings 26 (1995) 239.
[150] S. Fridrikh, C. Raquois, J.F. Tassin, S. Rezaiguia, J. Chim. Phys. 93 (1996) 941.
[151] B.E. Rodriguez, M.S. Wolfe, M. Fryd, Macromolecules 27 (1994) 6642.
[152] F.M. Horn, W. Richtering, J. Rheol. 44 (2000) 1279.
[153] T. Gisler, S.F. Schulz, M. Borkovec et al., J. Chem. Phys. 101 (1994) 9924.
[154] C.L.A. Berli, D. Quemada, Biorheology 38 (2001) 27.